Spike-timing-dependent plasticity can account for aftereffects of dual-site transcranial alternating current stimulation

Bettina C. Schwab[1,2], Peter König[1,3], Andreas K. Engel[1]

[1] Department of Neurophysiology and Pathophysiology, University Medical Center Hamburg-Eppendorf, Germany

[2] Institute for Advanced Study Berlin, Germany

[3] Institute of Cognitive Science, University of Osnabrück, Germany

Corresponding author

Bettina C. Schwab

Department of Neurophysiology and Pathophysiology, University Medical Center Hamburg-Eppendorf

Martinistraße 52, 20246 Hamburg, Germany

Email: b.schwab@uke.de

Abstract

Background: Transcranial alternating current stimulation (tACS), applied to two brain sites with different phase lags, has been shown to modulate stimulation-outlasting functional connectivity between the targeted regions.

Objective: Here, we test if spike-timing-dependent plasticity (STDP) can explain stimulation-outlasting connectivity modulation by dual-site tACS and explore the effects of tACS parameter choices.

Methods: Networks with two populations of spiking neurons were simulated. Synapses between the populations were subject to STDP. We re-analyzed resting-state EEG data to validate the model.

Results: Simulations showed stimulation-outlasting connectivity changes between in- and anti-phase tACS, dependent on both tACS frequency and conduction delays. Importantly, the model predicted that the largest effects would occur for short conduction delays between the stimulated regions, which agreed with experimental EEG connectivity modulation by 10Hz tACS.

Conclusions: STDP can explain connectivity aftereffects of dual-site tACS. However, not all combinations of tACS frequency and application sites are expected to effectively modulate connectivity via STDP. We therefore suggest using appropriate computational models and/or EEG analysis for planning and interpretation of dual-site tACS studies relying on aftereffects.

Keywords

Transcranial alternating current stimulation, Spike-timing-dependent plasticity, Electroencephalogram, Functional connectivity

Introduction

Transcranial alternating current stimulation (tACS) became a popular tool to modulate both oscillations and oscillatory connectivity in the brain [1]. As the measurement of extracellular potentials during tACS, including EEG and MEG, is hampered by large and hard-to-predict stimulation artifacts [2,3], measurement of stimulation-outlasting aftereffects turned into the standard [4,5]. So far, mechanisms mediating these aftereffects are not identified yet, but spike-timing-dependent plasticity (STDP) has been proposed as a candidate [6]. For EEG aftereffects in alpha- and beta-power, experimental evidence supports the involvement of STDP [7,8].

Applying electric fields with different phase lags to two different regions of the brain (dual-site tACS), seems ideal to exploit the plasticity of synapses between the targeted regions to induce aftereffects. Indeed, we [4] recently found that tACS at 10 Hz, applied in a focal montage to each hemisphere, transiently modulates stimulation-outlasting functional connectivity in the alpha range depending on the phase lag between the two applied electric fields. Specifically, functional connectivity increased after in-phase stimulation (phase lag zero) compared with anti-phase stimulation (phase lag π).

Here, we aim to test in a small computational model whether STDP can account for the experimentally observed connectivity changes after dual-site 10 Hz tACS. Furthermore, we vary tACS frequencies and synaptic delays between the stimulated regions to investigate which experimental settings maximize the size of effects in a given direction. We assume that tACS entrains at least some proportion of the targeted neurons, as shown in macaques [9,10], and validate the results of our simulations with existing EEG data [4].

Materials and Methods

We used small network models of spiking neurons to test the effect of different dual-site tACS protocols on connectivity changes due to STDP. A network consisted of two populations with 1000 Izhikevich neurons each [11] that followed the ordinary differential equations

$$\frac{dv}{dt} = 0.04v^2 + 5v + 140 - u + I$$
$$\frac{du}{dt} = 0.4a(bv - u)$$

with the auxiliary after-spike resetting

if $v \geq 30$, then $v \leftarrow c$ and $u \leftarrow u + e$.

Although the model is dimensionless, the variables v (transmembrane voltage) and t (time) can be interpreted in units of mV and ms, respectively. The membrane recovery variable u provides negative feedback to v. After v reaches the apex of a spike (30 mV), both v and u are reset. The parameters a, b, c, and e describe the time scale of u, the sensitivity of u to subthreshold fluctuations of v, the after-spike reset value of v, and the after-spike reset of u, respectively, which differ for neuron types. I represents input currents to the neuron, summing up the synaptic input from other neurons, random thalamic input, and tACS currents.

Depending on the network's architecture, neurons were synaptically coupled with fixed axonal conduction delays. After a spike in a presynaptic neuron, each postsynaptic neuron received an input sized w with delay d. In all networks, excitatory synapses between the two populations were subject to STDP. Connections between the populations were set to a low value w=0.01 in order to preserve the dynamics of each population but weakly couple the populations. Synaptic weight change Δw followed the rule

$$\Delta w(\Delta t) = \begin{cases} A_+ \cdot e^{-\Delta t/\tau_+}, & \Delta t > 0 \\ -A_- \cdot e^{\Delta t/\tau_-}, & \Delta t < 0 \end{cases}$$

with the difference between post- and presynaptic spike timing at the synapse $\Delta t = t_{post} - t_{pre}$ and the parameters $A_+ = 0.015$, $A_- = 0.007$, $\tau_+ = 13ms$, $\tau_- = 34ms$.

This rule was found experimentally by Froemke and Dan [12] in slices of rat visual cortex, layer 2/3, and is shown in Fig. 1A. Characteristics of this rule — in particular, $A_+ > A_-$ and $\tau_+ < \tau_-$ — have been corroborated by many other studies [13,14,15].

Importantly, synaptic weights will on average decrease in the case of independent Poisson firing ($\int_{-\infty}^{\infty} \Delta w(t)dt < 0$). In contrast, if Δt is small (say, distributed equally between $-\epsilon$ and ϵ with small, positive ϵ), average synaptic weights increase ($\int_{-\epsilon}^{\epsilon} \Delta w(t)dt > 0$). As a presynaptic spike at time t_1 arrives at the synapse at time $t_1 + d$, sharp synchrony of somatic pre- and postsynaptic spikes is expected to depress synapses (see Fig. 1A). However, spike synchrony with sufficient jitter may lead to a net potentiation (e.g., $\int_{-\epsilon-d}^{\epsilon-d} \Delta w(t)dt > 0$ for sufficiently small d and sufficiently large ϵ). For details on this mechanism, see [16].

Network 1:

First, we implemented a network without connections within each population (Fig. 1B), producing random firing in the absence of tACS, and tACS-phase-locked activity in the presence of tACS at various frequencies (Supplement A). All neurons were assigned b=0.2, c=-65mV, and e=8. The parameter a differed between neurons and was randomly set for each neuron following a Gaussian distribution A with mean 0.04 and standard deviation 0.015. Negative values of a were set to their absolute value. Every millisecond, 40 neurons of each population were chosen randomly to receive an input of $20a/\bar{A}$. Thus, the larger the parameter a of a neuron, the larger its thalamic input. This combination of the parameter a

and thalamic input led to a flat power spectrum (Fig. 1C) and a realistic distribution of firing rates (Supplement A). Each neuron was assigned 100 excitatory connections to random neurons of the other population with delay *d*. tACS was modeled as sinusoidal current input with amplitude 2 to all neurons, without a phase lag zero or π between the populations. Network 1 was simulated 100 times for two seconds; results were analyzed only for the last second.

Network 2:

Next, we adapted the network to a more realistic architecture that produces spontaneous alpha oscillations based on Izhikevich [17] (Fig. 2A,C). Each population was divided into an excitatory subpopulation of 800 neurons and an inhibitory subpopulation of 200 neurons. Excitatory neurons were assigned b=0.2, c=-65mV, e=8, and a drawn randomly from a Gaussian distribution with mean 0.04 and standard deviation 0.01, where negative values were set to their absolute value. Parameters of all inhibitory neurons were set to a=0.2, b=0.2, c=-65mV, and e=2. Connectivity within each population was similar to what was chosen in Izhikevich [17]: each excitatory neuron projected to 60 random neurons, which could be excitatory or inhibitory, with fixed weight w=6. Delays for those connections were distributed uniformly between 1ms and 10ms. Inhibitory neurons connected to 100 random excitatory neurons with fixed weight w=-5 and a delay of 1ms. This choice of connectivity and parameters led to realistic distributions of firing rates (Supplement B) and spontaneous emergence of alpha oscillations (Fig. 2B,D). Each excitatory neuron additionally connected to 100 random excitatory neurons of the other population with low weight w=0.01 (Fig. 2A). All synapses between the populations were subject to STDP. Each millisecond, 30 random neurons of each population received a thalamic input of size 30. tACS was modeled as

sinusoidal current input with amplitude 1 to excitatory neurons only. Network 2 was simulated for four seconds with tACS and aftereffects of three seconds with the latter being subject to analysis.

All simulations were run in MATLAB (The MathWorks Inc). Functional connectivity in Network 2 was simulated as the alpha-coherence (8-12 Hz) between the average transmembrane voltage of each population. To remove STDP, the learning rule was set to zero weight change for all time lags. To remove entrainment echoes, all transmembrane voltages were reset to their original values after tACS-offset. We also compared the simulations with our experimental data. Seven regions of interest (ROIs) in each hemisphere were targeted by tACS [4]. Thus, we were able to investigate 49 interhemispheric connections between stimulated ROIs, possibly differing in their conduction delays. EEG data were projected to source space using ELORETA and time series in each voxel were extracted as described in [4]. For all voxel pairs, we computed the cross-correlation function and extracted the absolute value of the time lag of its maximum. This lag was averaged for pairs between the same ROIs, and the average was correlated with the experimentally observed change in alpha-imaginary coherence. Permutation statistics were used to compute the p-value for this correlation (Supplement C).

Results

We first simulated two populations of randomly spiking neurons with weak connections subject to STDP (Network 1, Fig. 1A-C), which entrained to any tACS frequency in the range 10-50 Hz (Supplement A). 10 Hz tACS at different phase lags led to direction-specific changes in mean synaptic weights (Fig. 1D). As expected, weight changes were symmetric

only for phase lags zero ("in-phase stimulation") and π ("anti-phase stimulation"). We focused on these two special cases and, from then on, on average synaptic weights for all connections of e12 and e21. In particular, we were interested in the difference in average synaptic weight change between in- and anti-phase stimulation, which is shown in Fig. 1E for different combinations of stimulation frequency and synaptic delay. Clear effects in the positive direction direction — in-phase stimulation leads to an increase in synaptic weight compared with anti-phase stimulation — were found for low frequencies and short delays. With increasing frequency and delay, the effects diminished and eventually reversed.

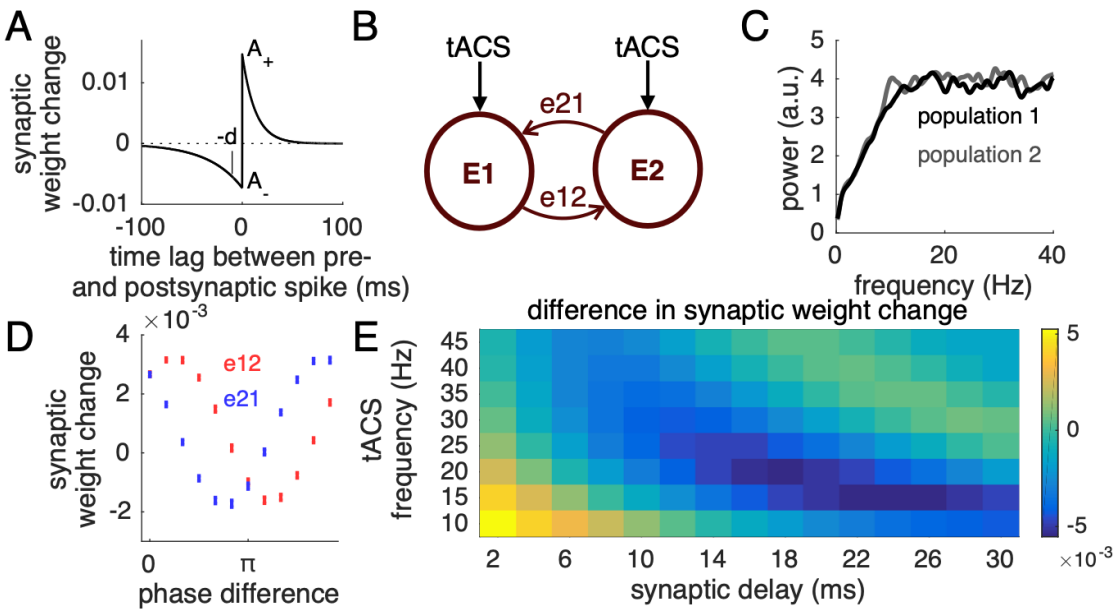

Fig. 1: A simple model of two spiking neuron populations (Network 1). A: STDP rule based on [12]. B: Network 1 consists of two populations with coupling only to neurons of the other population. C: Without stimulation, the network does not oscillate at a particular frequency. D: Stimulation of the two populations at different phase lags affects connectivity differently from population 1 to population 2 (e12) and vice versa (e21), shown here for *d*=10ms. At phase zero ("in-phase tACS") and phase π ("anti-phase tACS"), the system is symmetric, thus e12 and e21 show comparable changes in synaptic weights. E: The average difference in synaptic weight change between in- and anti-phase stimulation (mean ± standard deviation) depends on both tACS frequency and synaptic delay of connections e12 and e21. For low tACS frequencies and short delays, in-phase stimulation increases synaptic weights compared with anti-phase stimulation.

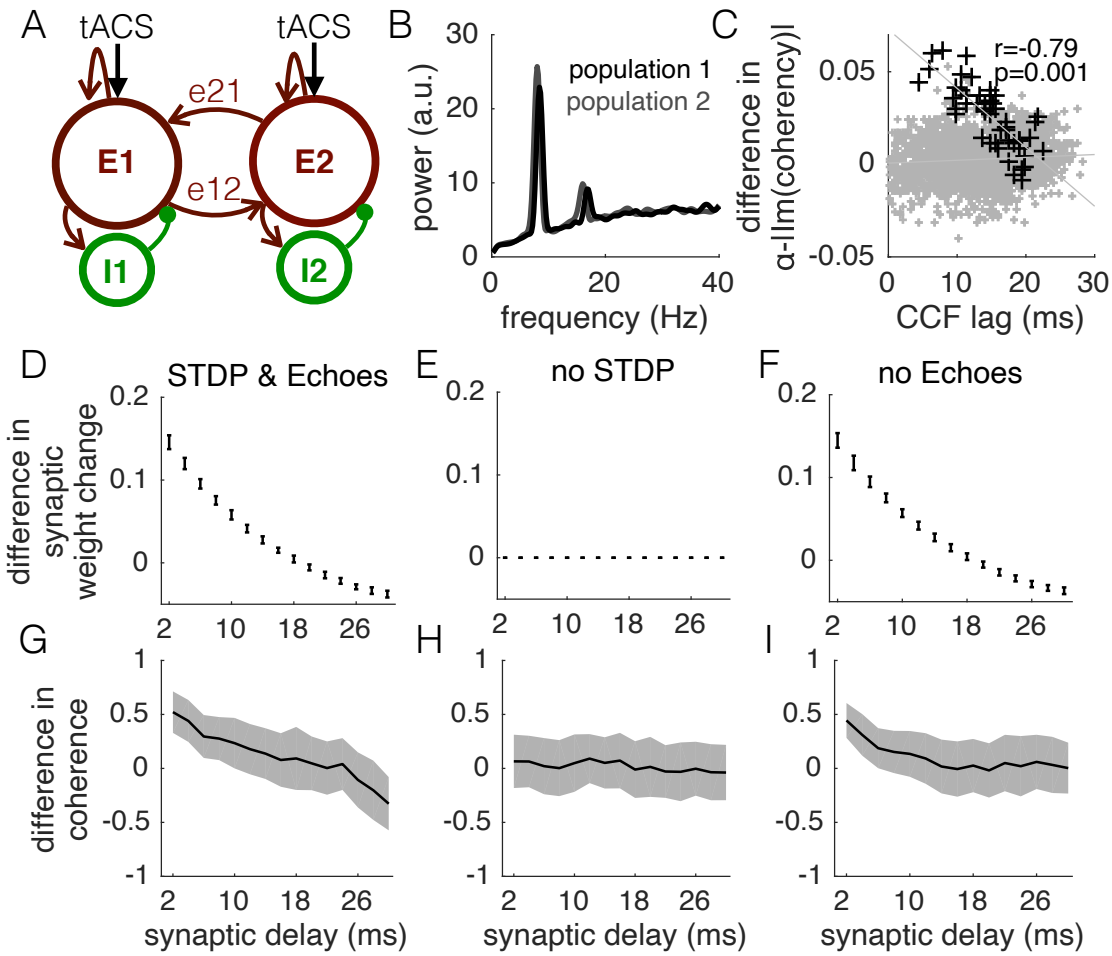

Fig. 2: Network 2, oscillating at alpha frequency due to realistic connectivity, confirms the results and is in agreement with experimental data. A: Architecture of Network 2: Each population consists of an excitatory and an inhibitory subpopulation. Excitatory neurons couple also between the two populations. B: Network 2 shows spontaneous alpha oscillations due to intrinsic coupling within each population. C: Experimental connectivity modulation dependent on the estimated conduction delay (CCF time lag). Stimulated pairs (black) show a negative relation between connectivity modulation and CCF time lag. D-F: Difference in average synaptic weight change between in- and anti-phase stimulation for the system with both STDP and entrainment echoes (D), with only entrainment echoes (E) and with only STDP (F). G-I: Respective differences in functional connectivity between in-and anti-phase stimulation.

Do our results depend on a realistic connectivity architecture and intrinsic oscillations? To answer this question, we extended the network with inhibitory subpopulations as well as intrinsic coupling (Network 2, Fig. 2A), which led to spontaneous alpha oscillations (Fig.

2B). Network 2 easily entrained to tACS at 10 Hz (Supplement B). Re-analysis of our experimental data revealed that the difference in functional connectivity between in- and anti-phase stimulation drops with the conduction delay between ROIs (Fig. 2C; for details, see Supplement D). In fact, our model predicted the same finding: differences in both structural connectivity (Fig. 2D) and functional connectivity (Fig. 2G) decreased with the conduction delay. At delay (20.2 ± 5.2) *ms*, the change in functional connectivity in our model was zero, in accordance with the experimental data ((22.8 ± 7) *ms*). Finally, we tested whether the change in functional connectivity actually related to the change in functional connectivity due to STDP, or was rather a result of entrainment echos. Removal of STDP (Fig. 2E,H) led to an absence of effects, while removal of entrainment echoes (Fig. 2F,I) only attenuated the effects. Therefore, in this model, STDP seems necessary to induce the experimentally observed effects, while entrainment echoes can further enhance effect sizes.

Discussion

With a small network model of spiking neurons, we demonstrated that aftereffects of dual-site tACS on connectivity at an intrinsic frequency of the network can be explained by STDP of synapses between the stimulated ROIs, possibly in combination with entrainment echoes. Critically, our model further suggests that these aftereffects depend on tACS frequency and synaptic delays, with the largest effects for low tACS frequencies and short delays. Re-analysis of our EEG data confirmed the dependence of connectivity modulation on the estimated delay, and thereby explained the heterogeneity of experimental results across ROI pairs. Indeed, most robust effects of dual-site tACS described in the literature have been found for theta frequencies [18]. In contrast, neural effects during tACS may be directly

related to entrainment of spiking [9,10] rather than plasticity of synapses and could therefore depend on different factors.

It is not the aim of this study to present a dynamic model with realistic cortical dynamics and effect sizes of tACS. Instead, the model relies on the assumption that spike *timing* is relevant for connectivity modulation. Thus, firing rate distributions, as well as the STDP rule, are critical and have to be adjusted to experimental data. Moreover, depending on factors like montage, amplitude, or brain state, tACS is expected to entrain only a small proportion of neurons. We simplify the situation by choosing tACS amplitudes large enough to entrain the majority of cells (Supplement B and C). Nevertheless, this discrepancy does not affect our conclusions, as the mechanism holds for neurons that are entrained.

Conclusion

Our model demonstrates that STDP can explain experimentally observed connectivity changes of dual-site stimulation at the network's intrinsic frequency. The direction of aftereffects is expected to depend on both tACS frequency and conduction delay between the targeted ROIs. Computational modeling and EEG connectivity analysis to estimate conduction delays may be used to predict the sign and magnitude of expected connectivity modulation by tACS to decrease variability and maximize effect sizes in future experimental studies.

Declarations of interest

None.

Acknowledgements

This work has been supported by DFG, SFB 936/project A3, and the Institute for Advanced Study Berlin.

References

[1] A. Antal and W. Paulus. Transcranial alternating current stimulation (tACS). *Frontiers in Human Neuroscience*, 7(317), 2013.

[2] N. Noury, J. F. Hipp, and M. Siegel. Physiological processes non-linearly affect electrophysiological recordings during transcranial electric stimulation. *NeuroImage*, 140(0):99–109, 2016.

[3] N. Noury and M. Siegel. Phase properties of transcranial electrical stimulation artifacts in electrophysiological recordings. *NeuroImage*, 158(0):406–416, 2017.

[4] B. C. Schwab, J. Misselhorn, and A. K. Engel. Modulation of large-scale cortical coupling by transcranial alternating current stimulation. *Brain Stimulation*, 12(5):1187–1196, 2019.

[5] M. Fiene, B. C. Schwab, J. Misselhorn, C. S. Herrmann, T. R. Schneider, and A. K. Engel. Phase-specific manipulation of rhythmic brain activity by transcranial alternating current stimulation. *Brain Stimulation*, 13(5):1254–1262, 2020.

[6] T. Zaehle, S. Rach, and C. S. Herrmann. Transcranial alternating current stimulation enhances individual alpha activity in human EEG. *PloS one*, 5(11):e13766, 2010.

[7] A. Vossen, J. Gross, and G. Thut. Alpha power increase after transcranial alternating current stimulation at alpha frequency (α-tACS) reflects plastic changes rather than entrainment. *Brain Stimulation*, 8(3):499– 508, 2015.

[8] M. Wischnewski, M. Engelhardt, M. A. Salehinejad, D. J. L. G. Schutter, M. F. Kuo, and M. A. Nitsche. NMDA receptor-mediated motor cortex plasticity after 20 Hz transcranial alternating current stimulation. *Cerebral Cortex*, 29(7):2924–2931, 2019.

[9] M. R. Krause, P. G. Vieira, B. A. Csorba, P. K. Pilly, and C. C. Pack. Transcranial

alternating current stimulation entrains single-neuron activity in the primate brain. *Proceedings of the National Academy of Sciences*, 116(12):5747–5755, 2019.

[10] L. Johnson, I. Alekseichuk, J. Krieg, A. Doyle, Y. Yu, J. Vitek, M. Johnson, and A. Opitz. Dose-dependent effects of transcranial alternating current stimulation on spike timing in awake nonhuman primates. *Science Advances*, 6(36), 2020.

[11] E. M. Izhikevich. Simple model of spiking neurons. *IEEE Transactions on Neural Networks*, 14(6):1569– 1572, 2003.

[12] R. C. Froemke and Y. Dan. Spike-timing-dependent synaptic modification induced by natural spike trains. *Nature*, 416(6879):433–438, 2002.

[13] G. Q. Bi and M. M. Poo. Synaptic modifications in cultured hippocampal neurons: dependence on spike timing, synaptic strength, and postsynaptic cell type. *Journal of Neuroscience*, 18(24):10464–10472, 1998.

[14] S. Song, K. D. Miller, and L. F. Abbott. Competitive Hebbian learning through spike-timing-dependent synaptic plasticity. *Nature Neuroscience*, 3(9):919–926, 2000.

[15] R. C. Froemke, M. M. Poo, and Y. Dan. Spike-timing-dependent synaptic plasticity depends on dendritic location. *Nature*, 434(7030):221–225, 2005.

[16] A. Knoblauch, F. Hauser, M. O. Gewaltig, E. Körner, and G. Palm. Does spike-timing-dependent synaptic plasticity couple or decouple neurons firing in synchrony?. *Frontiers in Computational Neuroscience*, 6(55), 2012.

[17] E. M. Izhikevich. Polychronization: computation with spikes. *Neural Computation*, 18(2):245–282, 2006.

[18] R. M. Reinhart and J. A. Nguyen. Working memory revived in older adults by synchronizing rhythmic brain circuits. *Nature Neuroscience*, 22(5):4820, 2019.

Supplements

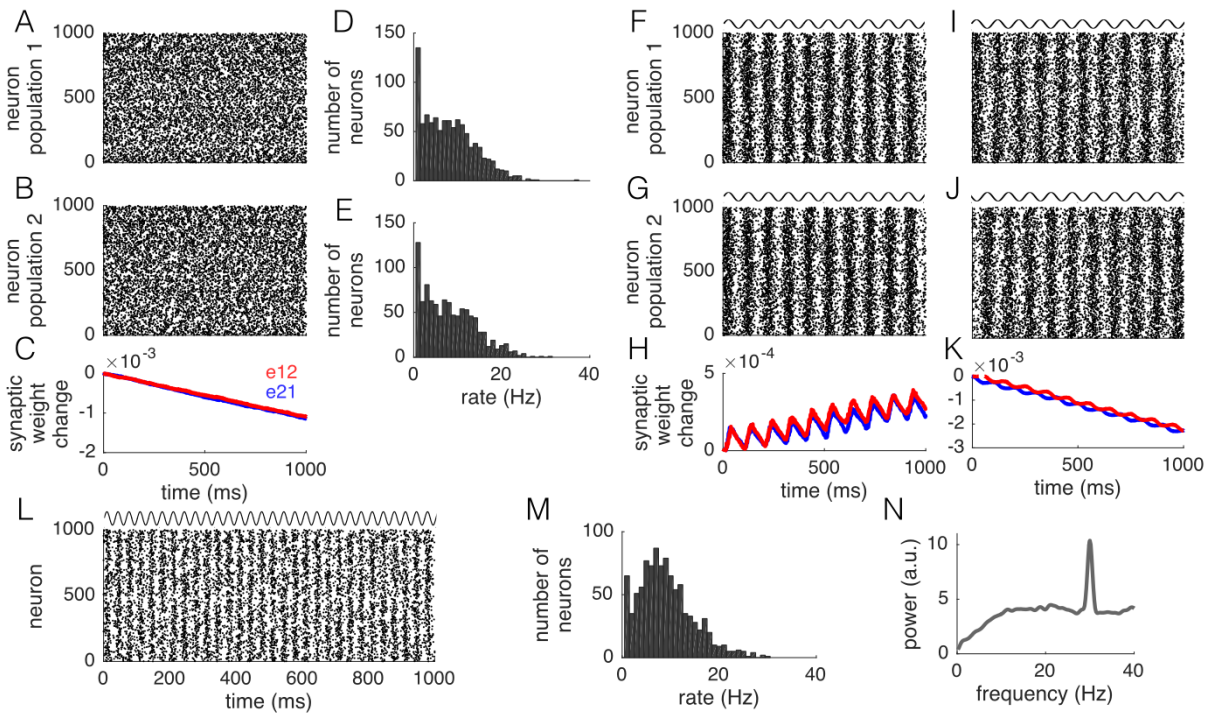

Supplement A. Examples for Network 1 with *d*=2ms. A,B: Firing patterns of neurons in population 1 and 2, respectively. No prominent oscillation is visible. C: Average synaptic weights of the connections between the two populations decrease. D, E: Firing rates of both populations are distributed in a wide range between 0 and 40 Hz. F, G: In-phase tACS leads to synchronous entrainment of the two population and a net potentiation of synaptic weights (H). I, J: In contrast, anti-phase stimulation entrains the two populations at phase lag π and induces a net depression of synaptic weights (K). L: Also tACS at higher frequencies entrains the network, here shown for 30 Hz. While firing rates are still distributed mainly around 10 Hz (M), average transmembrane voltages show a power peak at 30 Hz (N).

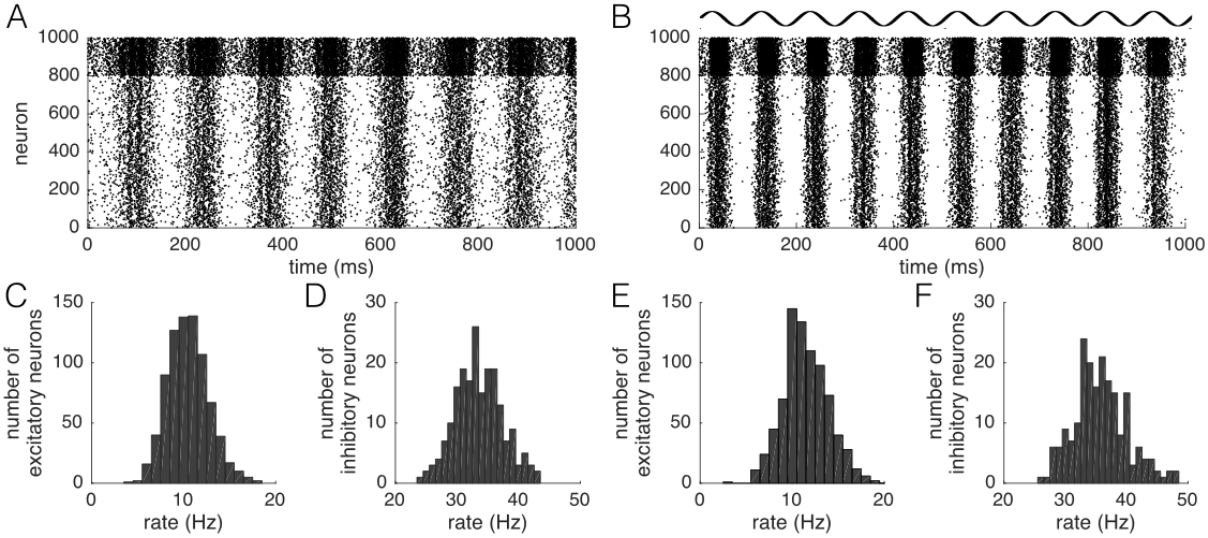

Supplement B. Examples for Network 2. A: Without tACS, the network spontaneously oscillates at around 8 Hz. B: 10 Hz tACS entrains the network to the stimulated frequency and phase. Firing rate distributions for excitatory (C, E) and inhibitory (D, F) neurons are comparable between the un-stimulated (C, D) and the stimulated (E, F) network.

Supplement C. Permutation statistics. We used permutation statistics to determine the p-value of the correlation between experimentally observed tACS effects and the estimated conduction delay (CCF lag) between the targeted regions (Fig. 1G). Each point in the scatter plot represents the connection between one ROI in the left hemisphere and one ROI in the right hemisphere. As ROIs contribute not only to one, but to multiple connections, values for both functional connectivity change and CCF lag are dependent on the other values. We therefore did not permute connections, but the seven ROIs, keeping the dependence between connections due to shared ROIs. The seven ROIs can be permuted in 7!=5040 different sequences. For each sequence, we computed the r-value ("permutation r"). The p-value could then be determined from percentiles of the distribution of permutation r-values.

Supplement D. Details and robustness of experimental results. To validate our model, we re-analyzed EEG data recorded in healthy participants before and after tACS [4]. Conduction delays between ROIs were approximated by the absolute time lag of the CCF peak. The differences in alpha-imaginary coherence between in- and anti-phase stimulation negatively correlated with the estimated conduction delay (r=-0.79, p=0.001) when restricting the analysis to the stimulated pairs (Fig. 2C, black crosses). We additionally analyzed the change in absolute coherence between ROIs that were not dominated by volume conduction. Domination of volume conduction was defined for ROI pairs with CCFs that were largest at absolute time lags below 1ms. Again, for stimulated pairs, condition differences in absolute coherence negatively correlated with the estimated conduction delay (r=-0.38, p=0.03),

although results were much more variable, possibly due to remaining effects of volume conduction. Finally, we considered an alternative measure for conduction delays between ROIs, the width of the largest CCF peak at half maximum. Similar to the previous measure (CCF lag), we found a negative correlation between this CCF width and differences in alpha-imaginary coherence ($r=-0.51$, $p=0.01$), further stressing the robustness of our findings.